Proceedings of the 2nd Marine Energy Technology Symposium
METS2014
April 15-18, 2014, Seattle, WA

PNEUMATIC PERFORMANCE OF A NON-AXISYMMETRIC FLOATING OSCILLATING WATER COLUMN WAVE ENERGY CONVERSION DEVICE IN RANDOM WAVES

by Diana Bull
Water Power Department, Sandia National Laboratories
E-mail: *dlbull@sandia.gov*

ABSTRACT

A stochastic approach is used to gain a sophisticated understanding of a non-axisymmetric floating oscillating water column's response to random waves. A linear, frequency-domain performance model that links the oscillating structure to air-pressure fluctuations with a Wells Turbine in 3-dimensions is used to study the device performance at a northern California deployment location. Both short-term, sea-state, and long-term, annual, predictions are made regarding the devices performance.

INTRODUCTION

An oscillating water column (OWC) wave energy converter is essentially a structure with a moonpool. The area above the moonpool is enclosed to create an air chamber that is open to atmosphere through a turbine. Thus as the incident waves cause pressure fluctuations in the air chamber the spinning turbine will produce power. A floating OWC requires that both the wave activated structure and the internal free surface elevation be modeled in a hydrodynamically coupled fashion since each absorbs power from the waves. It is the relative motion between the device and the internal free surface that produces pressure fluctuations.

A non-axisymmetric terminator design, the Backward Bent Duct Buoy (BBDB) [1], is modeled in this paper. This device is L-shaped with the opening to the ocean downstream from the wave propagation direction. Since the BBDB is non-axisymmetric it benefits from structurally cross-coupled resonant modes hydrodynamically combining with the internal free surface's resonant mode to expand the frequency range of efficient primary energy conversion. By linking the oscillating structure to the internal free surface with a control strategy implemented through the power conversion chain (PCC composed of turbine, generator, storage, and power electronics) additional increases in energy conversion are possible. [2]

In support of the DOE sponsored Reference Model Project[1], this paper applies a stochastic method [3] [4] to the BBDB to evaluate its performance, both pneumatic power and motions, within a northern California deployment wave climate. The linear response of the device in the short-term is governed by the wave spectrum describing the particular sea state. By deriving spectral densities of variables of interest (such as structural motion, pressure, and volume flow) from the device's response and the incident wave spectrum, a sophisticated understanding of the device in random waves can be quickly obtained. Furthermore, by combining these short-term responses with a long-term understanding of the deployment climate relevant predictions about the annual performance of the device are then made.

BBDB GEOMETRY

The geometry of the BBDB is the same as that described in [2] and [5]. Figure 1 illustrates the structural design and highlights key dimensions. The width of the device in the y-direction is 27 m. The majority of the device dimensions were

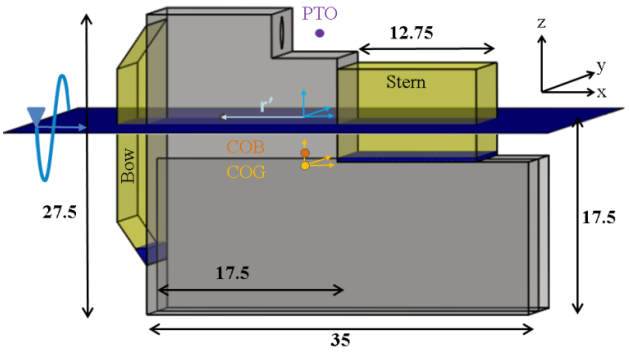

FIGURE 1. MODEL OF THE BBDB

[1] See http://energy.sandia.gov/rmp

selected based upon the conclusions of the following papers [6], [7], and [8]. This design is not optimized to reduce viscous losses or encourage weathervanning. The structural natural resonances of the device were selected to match the deployment climate, as highlighted later in the paper.

As indicated from the coordinate systems in Figure 1 a transformation vector is required to account for the velocity of the body at the center of the free surface in the global coordinate system (blue) due to body motions around the COG (as defined in the body coordinate system (gold)). The transformation in Eq. 1 relativizes the air-chamber results to the movements of the structure.

$$\boldsymbol{T} = [0 \quad 0 \quad 1 \quad 0 \quad -r' \quad 0]^{\mathrm{T}} \qquad 1$$

The structural properties of the device are summarized in Table 1.

Displaced Mass [kg]		2,024,657		
Structural Mass [kg]		1,808,944		
Bow Ballast Mass [kg]		22,072		
Stern Ballast Mass [kg]		123,641		
Power Conversion Mass [kg]		70,000		
Submerged Surface Area [m²]		4,251		
COG (x,y,z) [m]		0.00	0.00	-4.29
COB (x,y,z) [m]		0.00	0.00	-3.31
Free Surface Center (x,y,z) [m]		-5.12	0.00	0.00
Radius of Gyration at COG [m]	X	12.53	0.00	0.00
	Y	0.00	14.33	0.00
	Z	0.00	0.00	14.54

TABLE 1. STRUCTURAL PROPERTIES OF THE BBDB.

DEPLOYMENT CLIMATE

The spatial and temporal variability of ocean waves requires statistical treatment. Ocean waves, assumed as a Gaussian random process, are categorized by sea states which are valid for a short duration of time, typically 30 minutes to one hour. A sea state is minimally defined by a wave height, period, and spectral shape but it can also contain directional spreading characteristics. A spectrum defining a sea state, $S(\omega)$, is used to represent the variance of the ocean's surface distributed over radial frequencies, ω, and the shape determines the distribution of energy in the incident sea state. The spectrum is derived assuming ocean waves are stationary and random, following a Gaussian distribution.

Incident wave power for each sea state $i = T_p$ and $j = H_s$, assuming a discrete and unidirectional spectrum, is calculated according to [3]

$$J(T_p, H_s) = J_{ij} = \sum_k \rho g c_{g,k} S_{ij}(\omega_k) \Delta\omega_k. \qquad 2$$

In Eq. 2 ρ is the density of sea water (1025 kg/m³), g is acceleration due to gravity (9.81 m/s²), $c_{g,k}$ is the group velocity of the k^{th} frequency, $S_{ij}(\omega_k)$ is the variance density for the k^{th} discrete frequency of one-sided spectrum S_{ij} describing the sea state, and $\Delta\omega_k$ is frequency width of the discrete distribution centered at ω_k. J_{ij} is the total wave power per unit length (W/m); it is the energy flux through a vertical cylinder of unit diameter extending the full water depth.

Sea states allow the wave climate to be characterized for short durations of time, however in order to describe the deployment conditions that should be expected on an annual basis additional descriptions requiring many years of data are necessary. A joint-probability distribution (JPD) [9] is used to characterize the likelihood of a particular significant wave height, H_s, occurring with a particular period (either peak T_p, mean T_0, or energy T_e). The variables H_s, T_p, T_0, and T_e may all be derived from the properties of the spectrum describing the sea state (see [9] for further details).

Work by Cahill [10] exploring the occurrence of H_s versus the contribution of H_s to the total annual energy has shown that there is a separation in the distribution between these two metrics. This distinction indicates that a single metric in the form of an energy weighted occurrence may be better suited for optimizing a device design for a particular deployment climate.

The energy weighted occurrence is found by multiplying the occurrence of a variable, like $H_s(= j)$ or the period (either $T_p, T_0, T_e(= i)$), by the energy associated with that variable and normalizing by the total weighted energy to obtain a single metric that accounts for both the occurrence and the energy contribution of that variable. Eq 3 shows this analysis when evaluating the period

$$\zeta_i = \frac{\left(\sum_j JPD_{ij}\right)\left(\sum_j J_{ij}\right)}{\sum_{ij} JPD_{ij} J_{ij}}. \qquad 3$$

ζ_i is a vector of energy weighted occurrence of the period variable. The numerator determines the probability of a particular period occurring, regardless of its dependent variable H_s, as well as the energy associated with that period, as defined by Eq. 2. The combined factor is then weighted by the total weighted energy at the deployment site.

Northern California Deployment Location

The deployment site is approximately 3nmi from shore on a 60 m depth contour off the northern California coast near Eureka. Archived summary statistics from National Data Buoy Center (NDBC) 46212 buoy [11] were used to

Significant Wave Height, Hs [m] \ Peak Period, Tp [sec]	4.7	5.7	6.7	7.7	8.7	9.7	10.7	11.7	12.7	13.7	14.7	15.7	16.7	17.7	18.7
0.25	0.0	0.0	0.0	0.0	0.0	0.0	0.0	0.0	0.0	0.0	0.0	0.0	0.0	0.0	0.0
0.75	0.0	0.004	0.011	0.011	0.013	0.004	0.006	0.003	0.0	0.0	0.003	0.004	0.005	0.0	0.0
1.25	0.0	0.010	0.028	0.024	**0.046**	0.018	0.022	0.011	0.009	0.007	0.005	0.004	0.004	0.002	0.0
1.75	0.0	0.002	0.025	0.027	0.036	0.021	0.035	0.019	0.014	0.012	0.010	0.005	0.005	0.003	0.0
2.25	0.0	0.0	0.006	0.023	0.036	0.017	0.033	0.024	0.019	0.015	0.010	0.006	0.005	0.003	0.0
2.75	0.0	0.0	0.0	0.009	0.027	0.010	0.022	0.020	0.015	0.013	0.009	0.005	0.005	0.003	0.0
3.25	0.0	0.0	0.0	0.0	0.011	0.007	0.012	0.013	0.012	0.011	0.008	0.005	0.004	0.0	0.0
3.75	0.0	0.0	0.0	0.0	0.003	0.003	0.005	0.007	0.007	0.007	0.006	0.003	0.003	0.0	0.0
4.25	0.0	0.0	0.0	0.0	0.0	0.0	0.0	0.003	0.003	0.004	0.004	0.0	0.002	0.0	0.0
4.75	0.0	0.0	0.0	0.0	0.0	0.0	0.0	0.0	0.0	0.0	0.002	0.0	0.0	0.0	0.0
5.25	0.0	0.0	0.0	0.0	0.0	0.0	0.0	0.0	0.0	0.0	0.0	0.0	0.0	0.0	0.0
	4.0	**4.9**	**5.7**	**6.6**	**7.5**	**8.3**	**9.2**	**10.0**	**10.9**	**11.7**	**12.6**	**13.5**	**14.3**	**15.2**	**16.0**

Energy Period, Te [sec] $2\pi(m_{-1}/m_0)$

FIGURE 2. JPD FOR NDBC 46212 NEAR EUREKA CA.

generate the JPD of significant wave height, H_s, with peak period, T_p.

This data buoy is located in 40 m of water depth. Summary statistics spanning seven years (2004-2011) were used for this analysis. Although this data buoy has recorded the directional spectrums, only the significant wave height and peak period are used to characterize the deployment location. Figure 2 shows the 46212 JPD; the sum of all values within the JPD is one. The JPD is presented such that important aspects of the deployment climate may be quickly assessed: the numerical data is the occurrence, 95% of the climate is contained within the pink boxes, while 75% and 50% are contained within the yellow and green boxes respectively, the red highlighted values indicate the most common period for each H_s and the bolded red value indicates the most likely wave. It is clear from the shapes moving from 95% to 75% to 50% that the deployment location is predominantly a mixture of shorter wind waves and longer swell waves.

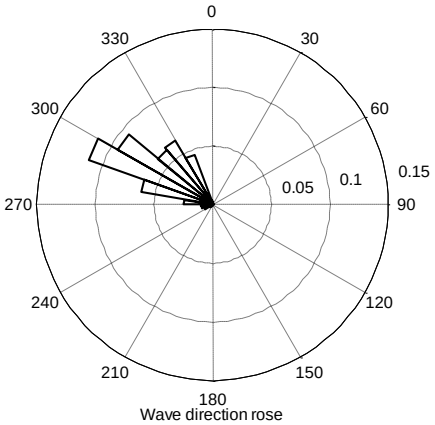

FIGURE 3. DIRECTIONAL WAVE ROSE FOR NDBC 46212 NEAR EUREKA CA.

The mean direction of the incident waves is narrowly distributed as is shown in Figure 3. Since the device is not axisymmetric, the incident wave direction will affect pneumatic power production. However, in this analysis, it is assumed that there is no directional spreading and that the incident spectrums are always in the x-direction. Assuming unidirectional, perpendicular waves allows the primary driver of the device performance, the frequency-dependence, to be effectually captured. This analysis additionally assumes a Bretschneider energy distribution. Since raw spectral data from this site has not been compared to the generalized Bretschneider spectrum the applicability of this spectral shape is unknown. With these two assumptions, the total weighted energy flux, or incident power, of 31.5 kW/m is found (the denominator of Eq. 3).

Figure 4 illustrates comparisons between the occurrence and the energy weighted occurrence for both H_s and T_p, see Eq. 3. The energy weighted occurrence is predictably shifted towards the larger and longer waves. It is convenient to view the two parameters, H_s and T_p, separately since devices are often tuned to frequencies as opposed to wave steepness's. Thus optimizing a design involves selecting structurally defined natural resonant frequencies to match the frequencies in the deployment climate. The effectiveness of this match can be quickly assessed by evaluating the capture width (the devices absorbed power divided by the incident power) against the energy weighted occurrence of the period variable.

As is shown in the second plot in Figure 4, the natural frequencies of the BBDB were chosen to align strongly with the energy weighted deployment climate. The coupled OWC resonance will be discussed in further detail later in the paper, while the structural resonances are derived using standard techniques. By choosing to match

the device's natural resonances to the energy weighted frequencies in the deployment climate, the design will be capable of producing more power than if it were designed to solely match the occurrence.

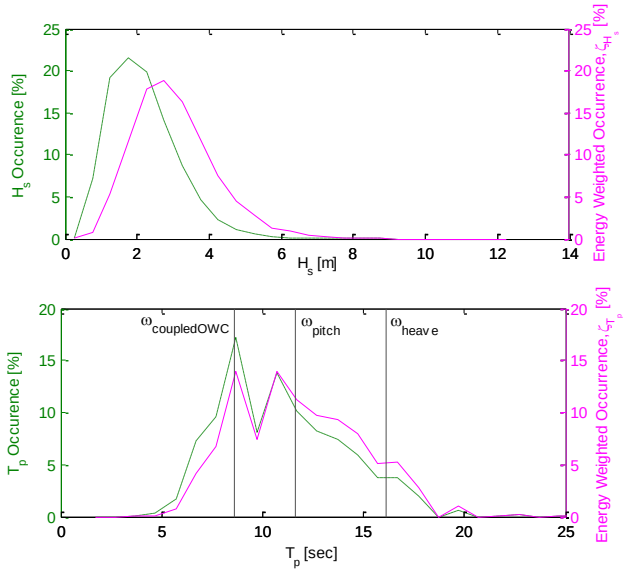

FIGURE 4. COMPARISON OF OCCURRENCE TO ENERGY WEIGHTED OCCURRENCE FOR EUREKA CA.

MONOCHROMATIC PNEUMATIC PERFORMANCE MODEL

The monochromatic performance model based on linear potential flow theory was first presented in [2] and is summarized here. This model accounts for hydrodynamic coupling between the structure and the air column. Additionally, the structure is linked to the air column through a control parameter R_{load}.

Floating OWCs require that both the wave activated body and the contained water column are modeled in a hydrodynamically coupled fashion since each absorbs power from the waves. In other words, each can be described to have excitation ($\boldsymbol{f}$ (structure) and q (free surface)) and radiation ($\boldsymbol{Z}$ (structure and Y (free surface)) solutions as well as a coupling term to unite them ($\boldsymbol{H}$). In this formalism bolded quantities are matrices or column vectors. The hydrodynamic properties of the floating structure can be obtained directly from WAMIT v6.4 [12], a Boundary Element Method (BEM) solver. The hydrodynamic properties of the internal free surface are determined implicitly through the use of reciprocity relations. [13] [14] [15] [2] By modeling the internal pressure distribution in this manner, no approximations are required as the full radiation potential is resolved through the array of field points.

Determination of the internal free surface hydrodynamic terms is detailed in [2]. Further, the frequency dependence of these terms for the BBDB detailed in this paper is shown for wave frequencies spanning 0 to 2.5 rad/s in 0.01 rad/s intervals assuming infinite depth. An array of 231 field points defining the interior free surface allows hydrodynamic parameters relating to the fluctuating air-pressure within the BBDB to be calculated.

For grounded OWC's the natural resonance of the water column is solely dependent upon the length and surface area of the water column [16] [17]. This location is often referred to as the "piston" resonance of the OWC. However, by hydrodynamically coupling the structural resonant modes with the internal free surface, the location of the internal free surface resonant mode can migrate significantly depending upon the structural resonant modes. This phenomena is first described in [2]. The coupled OWC natural resonance shown in Figure 4 at 8.6 sec has migrated from a "piston" location of 13.7 sec as described in [2].

Once the coupled wave-structure-OWC dynamics are understood through the hydrodynamic parameters, a performance model must then be constructed to link the wave-activated dynamics to the controls implemented through the PCC. In this performance model a linear relationship between pressure and flow, consistent with a Wells Turbine, is assumed. The slope between pressure and flow, R_{load}, can be altered *in situ*. The pneumatic power available to the PCC is dependent upon R_{load}. Air compressibility is modeled assuming a linearized isentropic relationship.

The linked governing equations in response to wave amplitude A are most readily understood in matrix notation as follows:

$$\begin{pmatrix} \boldsymbol{f} \\ q \end{pmatrix} A = \begin{pmatrix} \boldsymbol{Z}_i & -\boldsymbol{H}_i \\ \boldsymbol{H}_i^T & Y_i + \dfrac{1}{R_{load}} \end{pmatrix} \begin{pmatrix} \boldsymbol{u} \\ p \end{pmatrix} \qquad 4$$

where:

$$\boldsymbol{Z}_i = \boldsymbol{b} + \boldsymbol{b}_{vis} + i\omega\left(\boldsymbol{m} + \boldsymbol{a} - \frac{(\boldsymbol{C}+\boldsymbol{K})}{\omega^2}\right), \qquad 5$$

$$\boldsymbol{H}_i = \boldsymbol{H} + \boldsymbol{T}\boldsymbol{S}, \text{ and} \qquad 6$$

$$Y_i = \left(G + \frac{1}{R_{vis}}\right) + i\left(B + \frac{\omega \forall_o}{\gamma p_{atm}}\right). \qquad 7$$

In Eq. 4 the velocity of the body $\boldsymbol{u}$ and the pressure in the internal air chamber p are united through the hydrodynamic coupling term $\boldsymbol{H}_i$. $\boldsymbol{H}$ is modified by the transformation vector $\boldsymbol{T}\boldsymbol{S}$, S is the surface area, to account for the pressure-volume flow that occurs due to the velocity of the body at the center of the free surface.

The velocity Response Amplitude Operator (RAO), the velocity of the body per unit wave

amplitude ($\boldsymbol{u}/_A$) for each incident wave frequency, is further determined through traditional hydrodynamic terms: the radiation damping $\boldsymbol{b}$ and added mass $\boldsymbol{a}$, the excitation force $\boldsymbol{f}$, as well as the restoring forces $\boldsymbol{C}$, mooring forces $\boldsymbol{K}$, and mass of the structure $\boldsymbol{m}$. The mooring restoring force is obtained from the mooring design detailed in [5]. The design was found to act linearly for excursions of $\pm$5m in the surge, sway, and heave directions. The magnitudes of the restoring forces are: 55.5 kN in surge, 6.1 kN in sway, and 7.5 kN in heave. Additionally, linearized, constant, and diagonal viscous losses are applied to the structure through the term $b_{vis} = 0.02(2\sqrt{M_{tot}c_{tot}})$. M_{tot} is the physical mass in combination with the infinite frequency added mass and c_{tot} is the total restoring force (hydrostatic plus mooring).

The pressure RAO is determined through coupling and linking, as well as: the radiation susceptance B and conductance G (analogs of the structural radiation terms) as well as the excitation volume flow q. Air compressibility is specified through the initial volume $\forall_o$, the ratio between the constant-pressure and constant-volume specific heats for air $\gamma = 1.4$, and the atmospheric pressure p_{atm}. As for the structure, linearized viscous losses in the air chamber are accounted for through the term $R_{vis}^{-1} = 0.01(\max(G))$. The relative volume flow RAO may be calculated as:

$$Q_T = qA - Y_i p - \boldsymbol{H}_i^T \boldsymbol{u} = \frac{p}{R_{load}}. \qquad 8$$

The pneumatic power is the product of the relative pressure in the air-chamber and the relative volume flow [13]

$$\langle P \rangle = \overline{p(t)Q_T(t)} = \frac{1}{2} Re\{pQ_T^*\}. \qquad 9$$

The pressure, p, is found through solution of Eq. 4 and is the relative pressure resulting from both the movements of the structure as well as the water column.

In monochromatic waves, the average pneumatic power simplifies to

$$\langle \mathrm{P} \rangle = \frac{1}{2}\frac{1}{R_{load}}|p|^2. \qquad 10$$

An analytic solution for optimal form of the frequency dependent resistive damping can be found for monochromatic waves. As first presented in [2], the optimal resistive damping is:

$$R_{l_{opt}} = (|Y_i + \boldsymbol{H}_i^T \boldsymbol{Z}_i^{-1} \boldsymbol{H}_i|^2)^{-\frac{1}{2}}. \qquad 11$$

PNEUMATIC PERFORMANE MODEL IN RANDOM WAVES

The monochromatic BBBD performance model must be expanded to understand how the device will respond to random waves. Since the response of the device is linear, the spectral response of the device will follow the spectrum describing the incident climate. This spectral understanding will allow for statistical understanding of the devices response in random waves.

Optimal Resistive Loading

There is no closed form optimization procedure for R_{load} when evaluating the spectral response like there is for monochromatic waves (see Eq. 11). The optimal R_{load} for each sea state is thus found through numeric optimization. This procedure assumes that only one R_{load} can be applied for the duration of the sea state and hence one R_{load} is applied across all frequencies.

In this case, the devices response in each sea state was obtained for R_{load} spanning 1-200 Pa/m^3/sec in increments of 1 Pa/m^3/sec. The optimal value is the one that produces the largest average power in the sea state (as described below in Eq. 15). There are more advanced algorithms that will more accurately identify the true maximum power (see [18] for example), however they were not utilized in this study. Figure 5 shows the results of the optimization.

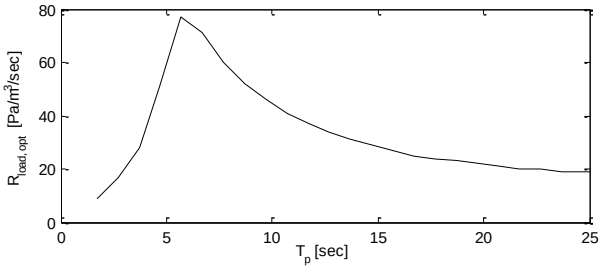

FIGURE 5. OPTIMAL RLOAD FOR TP

Spectral Density

In order to transform from monochromatic to spectral response, relevant RAO's and the wave spectrum $S(\omega)$ that the device will be subject to are required. The variables' RAO will not apply $R_{l_{opt}}$ as specified in Eq. 11. Instead, a single R_{load}, as determined by Figure 5, must be applied across all frequencies in the RAO. The response spectrum, S_R, for any variable R can then be obtained through the following calculation [3]

$$S_R(\omega) = [\mathrm{RAO}(\omega)]^2 S(\omega). \qquad 12$$

The RAO has units of response per unit wave amplitude (i.e. Pa/m, N/m, etc.), the wave spectrum has units of (height)^2-time (i.e. m^2-s), and hence the response spectrum will have units

of (response unit)²-time (i.e. Pa²-s, N²-s, etc.). Figure 6 below illustrates the required inputs and the resulting spectral density for the volume flow in the BBDB.

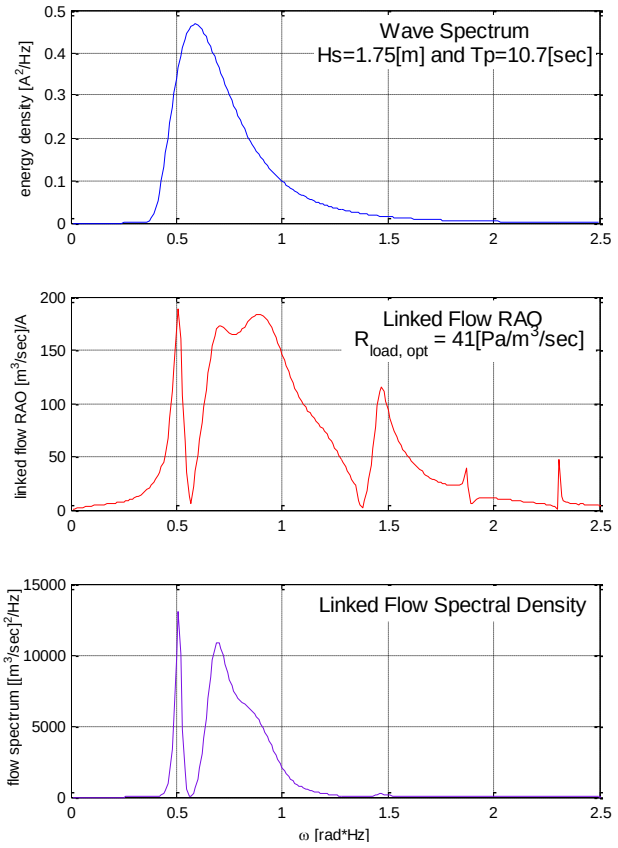

FIGURE 6. FLOW SPECTRAL DENSITY CALCULATION.

Relevant statistical parameters can be calculated from the variable's spectral density since the structural response will also be stationary and random, following a Gaussian distribution. The root-mean-square (RMS) and significant values, as shown in Eq.'s 13 and 14 respectively, can be calculated for any variable R.

$$R_{RMS} = \sqrt{\int S_R(\omega)d\omega} = \sqrt{m_0} \qquad 13$$

$$R_s = 2\sqrt{\int S_R(\omega)d\omega} = 2\sqrt{m_0} \qquad 14$$

Above, m_0 is the zeroth moment of the spectral density. The integrals in Eq. 13 and 14 are approximated using trapezoidal summation over the frequency range defined by the WAMIT run.

The average absorbed power in the sea state is calculated using the spectral density calculation for either the flow or the pressure in the air chamber. Eq. 15 below shows the calculation using flow.

$$\langle P_{ij} \rangle = R_{load,i} \int Q_{T,ij}(\omega)^2 S_{ij}(\omega)d\omega \qquad 15$$

Alternatively, the average power can be obtained through the product of the RMS pressure and flow, as derived from the spectral density. This absorbed power is often referred to as the pneumatic power for OWC devices.

Since the device is modeled linearly in the frequency domain, increasing H_s for a particular T_p multiplicatively increases $\langle P \rangle$. Hence, the capture width is often used to represent the response of a device to incoming seas. This measure of efficiency is obtained through a ratio of absorbed power in a particular sea state to the incident wave power in that sea state:

$$\chi_{w,i} = \frac{\langle P_i \rangle}{J_i}. \qquad 16$$

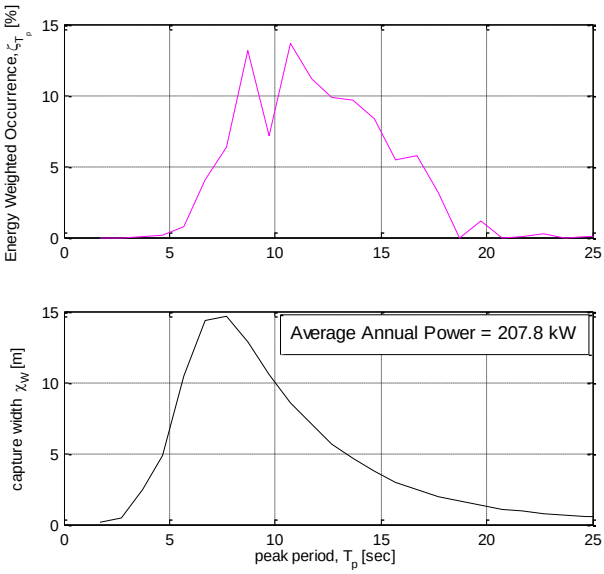

FIGURE 7. ENERGY WIEGHTED OCCURRENCE AND SPECTRAL CAPTURE WIDTH OF BBDB.

The spectral capture width is a function of T_p and when compared to ζ_{T_p} allows the device designer to quickly assess the compatibility between device performance and energy weighted deployment climate characteristics. Figure 7 illustrates this comparison.

Comparison of the spectral capture width χ_w with ζ_{T_p} shows that the device may be designed more effectively for this control strategy by instituting changes that would shift the peak of χ_w towards longer periods. This finding is interesting since the natural periods shown in align so well with ζ_{T_p}. This is likely due to the control strategy implemented in this model: a constant R_{load} for all frequencies in a sea state.

ANNUAL PNEUMATIC PERFORMANCE AT DEPLOYMENT LOCATION

Long-term performance estimates for a device are obtained by combing results from the spectral treatments with the JPD for the deployment site. For instance the average annual pneumatic power (AAP) for the device can be obtained according to Eq. 17.

$$\mathrm{AAP} = \sum_{ij} JPD_{ij} \langle P_{ij} \rangle \qquad 17$$

Here, the power weighted matrix is obtained by multiplying the average power produced in each sea state by the probability of that sea state occurring. The sum of the power weighted matrix results in the average annual power production at the deployment location. This procedure can be followed to obtain annual estimates of any variable: annual significant flow, annual RMS pressure, annual RMS pitch angle, etc.

Table 2 highlights annual estimates for key variables describing the dynamics of the device. As can be seen not only are annual estimates of the power available, but also estimates of device motion. These types of estimates can give the designer a sense for how the device will be responding in the deployment climate.

Variable		RMS (Eq. 13)	Significant (Eq. 14)
Pneumatic Power	kW	207.8	--
Pneumatic Energy Production	MW-hr	1820	--
Capture Width	m	8.89	--
Pressure	Pa	2728	5456
Flow	m^3/sec	66.2	132.5
Heave	m	0.43	0.87
Pitch	deg	2.9	5.7

TABLE 2. ANNUAL ESTIMATES OF PERFORMANCE.

Following the work of [19], evaluation of performance measures can further illuminate the device response in the deployment climate for the designer. The absorbed energy per displaced mass for this device is 0.90 MW-hr/tonne; the average annual pneumatic energy production is given in Table 2 while the displaced mass is given in Table 1. The absorbed energy per surface area is 0.43 MW-hr/m^2; the average annual pneumatic energy production is given in Table 2 while the (submerged) characteristic surface area is given in Table 1. The capture width ratio, the ratio of the capture width presented in Table 2 to the width of the device (27 m), is 33%.

The BBDB design presented in [19] uses the model presented in [15]. As noted in Eq. 12 of [2], the wrong non-dimensionalization was used in the performance model developed in [15]. Hence the results presented here for the performance measures should not be directly compared to the results presented for the BBDB in [19]. However, it is instructive to compare these results to the other devices.

The absorbed energy per displaced mass compares well to the average value found in [19] of 1MW-hr/tonne. The absorbed energy per surface area is approximately half of the average value found in [19] of 1.0 MW-hr/m^2 across the device designs. It is not clear why there is such a divergence on this metric. However, as stated above this device was not optimized to reduce viscous losses or encourage weathervanning, hence these changes may affect this particular metric.

CONCLUSIONS

A stochastic approach was applied to a floating non-axisymmetric OWC (a BBDB) in order to determine its response to random waves. This device produces 208kW of average annual pneumatic power in a northern CA climate resulting in an average annual capture width ratio of 33%. In general this device's performance measures are on par with those presented for other WEC devices in [19].

A methodology was presented to optimize a devices performance in a deployment climate. This procedure is first comprised of determining the peak periods energy weighted occurrence. Secondly the device should then be designed to align the natural resonance(s) with the energy weighted distribution. Although, the spectral capture width should be compared to the energy weighted occurrence of the period to ensure that the device's response is optimally aligned with the climate. For this device, Figure 7 shows that although the natural resonances align with the deployment climate, the spectral capture width does not maximally overlay with the energy weighted occurrence of the period.

Since most WECs have frequency-dependent and directionally-dependent performance characteristics, it is important to accurately determine the spectral shape and directional characteristics at the deployment location. In this analysis a unidirectional Bretscheinder spectrum was used. This simplified approach to estimating the incident wave power will not result in accurate predictions of BBDB response when deployed off the coast of northern CA.

Pneumatic power must be converted to mechanical and then electrical power to enter the electric grid. Hence, this work must be expanded to consider the losses incurred through the Wells Turbine, generator, and power electronics (see

[20] for this expansion). It is well known that the Wells Turbine does not possess high efficiency over a broad flow rate range, hence it is expected that the average annual electric power will be substantially less than the average annual pneumatic power. Further, optimization for mechanical power, as opposed to pneumatic power, is expected to result in a distinct R_{load} profile.

ACKNOWLEDGEMENTS

Vince Neary offered helpful comments while considering the energy weighted occurrence. This work was funded by the Department of Energy's Wind and Water Power Technologies Office. Sandia National Laboratories is a multi-program laboratory managed and operated by Sandia Corporation, a wholly owned subsidiary of Lockheed Martin Corporation, for the U.S. Department of Energy's National Nuclear Security Administration under contract DE-AC04-94AL85000.

REFERENCES

[1] Y. Masuda, T. Yamazaki, Y. Outa, and M. McCormick, "Study of backward bent duct buoy," in *OCEANS'87*, 1987, pp. 384–389.

[2] D. Bull and E. Johnson, "Optimal Resistive Control Strategy for a Floating OWC Device," in *Proceedings of the 11th European Wave and Tidal Energy Conference*, Aalborg, Denmark, 2013.

[3] Subrata Chakrabarti, *Hydrodynamics of Offshore Structures*. Boston, MA: WIT Press, 1987.

[4] A. F. d. O. Falcão and R. J. . Rodrigues, "Stochastic modelling of OWC wave power plant performance," *Applied Ocean Research*, vol. 24, no. 2, pp. 59–71, Apr. 2002.

[5] D. Bull and P. Jacob, "Methodology for creating nonaxisymmetric WECs to screen mooring designs using a Morison Equation approach," in *OCEANS '12. "Harnessing the Power of the Ocean". Proceedings*, Hampton Roads, VA, 2012, pp. 1 –9.

[6] Y. Imai, K. Toyota, S. Nagata, T. Setoguchi, and M. Takao, "An Experimental Study on Generating Efficiency of a Wave Energy Converter" Backward Bent Duct Buoy," presented at the EWTEC.

[7] M. Suzuki, T. Kuboki, S. Nagata, and T. Setoguchi, "Numerical Investigation of 2D Optimal Profile of Backward-Bent Duct Type Wave Energy Converter," *J. Offshore Mech. Arct. Eng.*, vol. 133, no. 4, Nov. 2011.

[8] D. Hong, S. Hong, and S. Hong, "Numerical study on the reverse drift force of floating BBDB wave energy absorbers," *Ocean engineering*, vol. 31, no. 10, pp. 1257–1294, 2004.

[9] Michel K. Ochi, *Ocean Waves: The Stochastic Approach*. Cambridge University Press, 1998.

[10] B. Cahill and T. Lewis, "Wave Energy Resource Characterization and the Evaluation of Potential Wave Farm Sites," presented at the IEEE/MTS Oceans, 2011.

[11] National Oceanic and Atmospheric Administration and US Department of Commerce, "National Data Buoy Center." Available: http://www.ndbc.noaa.gov/. [Accessed: 27-Jun-2013].

[12] *WAMIT v6.4*. Chestnut Hill, Massachusetts: WAMIT, Inc.

[13] Johannes Falnes, *Ocean Waves and Oscillating Systems*. New York: Cambridge University Press, 2002.

[14] C. H. Lee and F. G. Nielson, "Analysis of oscillating-water column device using a panel method," presented at the 11th International Workshop on Water Waves and Floating Bodies, Hamburg Germany, 1996.

[15] Kurniawan, A, Hals, J, and Moan, Torgeir, "Modeling And Simulation Of A Floating Oscillating Water Column," in *Proceedings of the ASME 2011 30th International Conference on Ocean, Offshore and Arctic Engineering*, Rotterdam, The Netherlands, 2011.

[16] Fukuda, K., "Behaviour of water in vertical well with bottom opening of ship, and its effect on ship motions," *Journal of Naval Architects of Japan*, vol. 141, pp. 107–122, 1977.

[17] Y. Wei, J. Yang, G. Chen, and Z. Hu, "The Research of Moonpool Size Effect on the Hydrodynamic Performance of FDPSO," in *Proceedings of the ASME 2011 30th International Conference on Ocean, Offshore and Arctic Engineering*, Rotterdam, The Netherlands, 2011, pp. 459–467.

[18] D. Sarkar, E. Renzi, and F. Dias, "Wave power extraction by an oscillating wave surge converter in random seas," in *ASME 2013 32nd International Conference on Ocean, Offshore and Arctic Engineering*, 2013.

[19] Babarit, A., Hals, Jorgen, Muliawan, M.J., Kurniawan, A, Moan, Torgeir, and Krokstad, J., "Numerical benchmarking study of a selection of wave energy converters," *Renewable Energy*, vol. 41, pp. 44–63, May 2012.

[20] C. Smith, D. Bull, S. Willits, and A. Fontaine, "Optimization and average annual power predictions of a Backward Bent Duct Buoy oscillating water column device using a Wells Turbine," in *Proceedings of the 2nd Marine Energy Technology Symposium*, Seattle, WA, USA, 2014.